La mer 43 : 49-59, 2005
Société franco-japonaise d'océanographie, Tokyo

Deep Western Boundary Current along the eastern slope of the Kerguelen Plateau in the Southern Ocean: observed by the Lowered Acoustic Doppler Current Profiler (LADCP)

Yoshihiro NARUMI*, Yuji KAWAMURA**, Tomoko KUSAKA*, Yujiro KITADE* and Hideki NAGASHIMA*

Abstract : The Deep Western Boundary Current (DWBC) is considered to flow northwestward along the eastern slope of the Kerguelen Plateau in the Southern Ocean. SPEER and FORBES (1994) estimated the volume transport of DWBC at 6 SV (1SV=10^6 m^3/s) northwestward based on the assumption of a level of no motion at 2500 dbar depth. However, there is no evidence of an existence of such a level in the deep sea over the plateau. To clarify the transport of the current, we tried to observe the current profile by using the Lowered Acoustic Doppler Current Profiler (LADCP) and CTD at a section that crosses isobaths of the plateau. The cross sectional transport is estimated at 10 SV northwestward from the LADCP data, and is about 1.7 times larger than that by SPEER and FORBES (1994) . The geostrophic transport is estimated from the CTD data by adjusting a reference level in order that the total transport coincides with that calculated from the LADCP data. The baroclinic and barotropic transports are estimated at 5 SV southeastward and 15 SV northwestward, respectively.

Keywords *: LADCP, the Kerguelen Plateau, Deep Western Boundary Current (DWBC), Geostrophic Transport*

1. Introduction

The Antarctic Bottom Water (AABW) is produced around the Antarctica. The main three areas in which AABW is produced are considered to be the Weddell-Enderby Basin, the South Pacific Basin and the South Indian Basin. The origin of AABW in the South Indian Basin is recognized as the continental shelf and continental slope is located at the region off Adélie Land. The behavior of this water is influenced by topographical effect of ocean floor, e.g. the Princess Elizabeth Trough and the Kerguelen Plateau.

The AABW in the source region off the Adélie Land (ADLBW: Adélie Land Bottom Water) flows westward along the continental slope (e.g. MANTYLA and REID, 1995; ORSI *et al.*, 1999; BINDOFF *et al.*, 2000), and is prevented by the Princess Elizabeth Trough and some of this turn northwestward along the Kerguelen Plateau. SPEER and FORBES (1994) investigated the Deep Western Boundary Current (DWBC) along the eastern flank of the Kerguelen Plateau from its geostrophic shear and water mass properties. Then this water mass flows to the north of the Antarctic Divergence, and turns eastward due to the influence of the Antarctic Circumpolar Current (ACC) and some of this water forms recirculation (BINDOFF *et al.*, 2000). ORSI *et al.* (1999) also suggested these flow fields based on the horizontal density distribution of the Southern Indian Ocean. SPEER

* Department of Ocean Sciences, Tokyo University of Marine Science and Technology, 4-5-7 Konan, Minatoku, Tokyo 108-8477, Japan
** Present address: Center for Marine Environmental Studies, Ehime University, 2-5 Bunkyotyo, Matsuyama, Ehime 790-8577, Japan

Corresponding to Authors
Telephone: 03-5463-0380 FAX: 03-5463-0378 E-mail: od02109@edu.s.kaiyodai.ac.jp

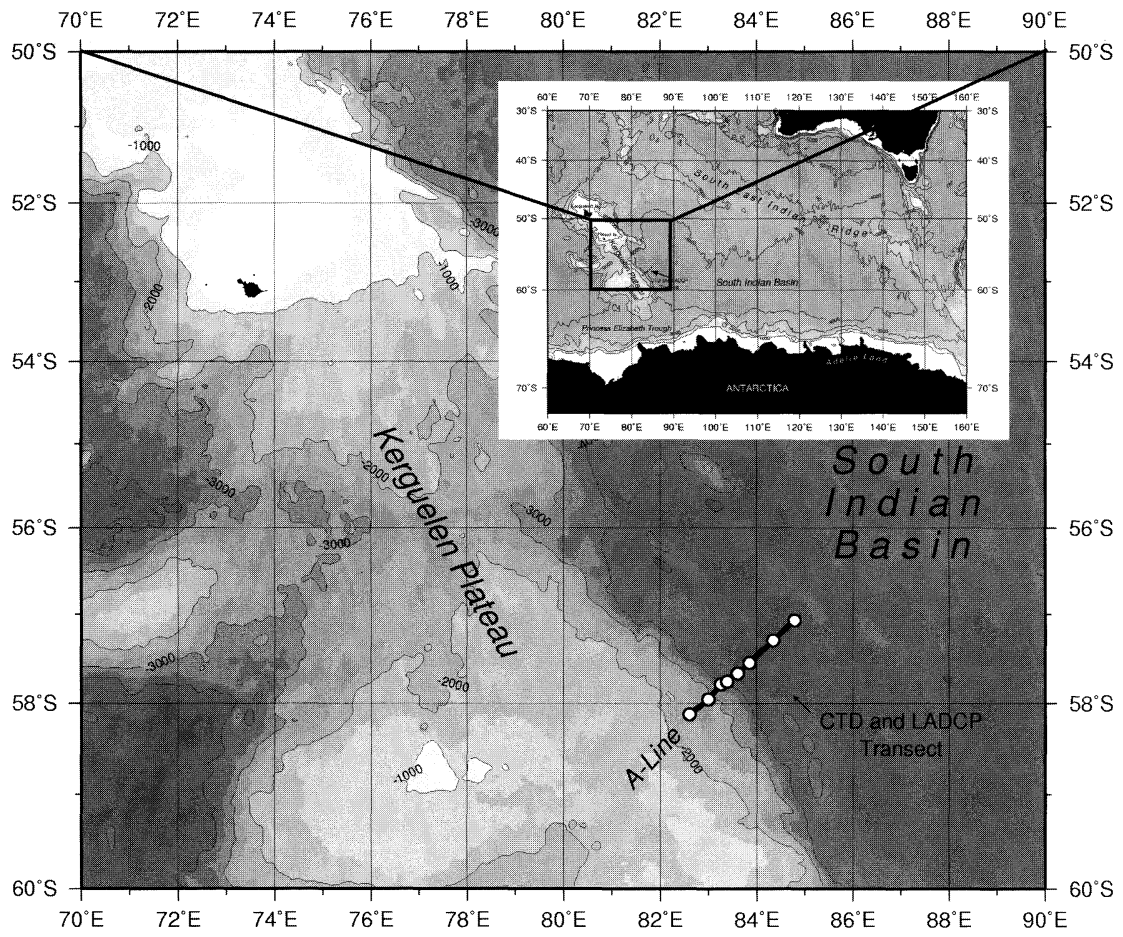

Fig. 1. Locations of CTD and LADCP observation stations (circles) along A-line (Bold line). Contour obtained from ETOPO2 bathymetric data are depicted every 1000 m. Numerals attached to contour stand for depth in m. Shaded areas show depth less than 500 m.

and FORBES (1994) estimated the geostrophic transport of bottom water at 6.0 SV northwestward from the hydrographic observation. The estimated geostrophic transport of DWBC is about 48.9 SV northwestward on the bases of LADCP referenced velocity (DONOHUE *et al.*, 1999). But they don't mention about the current profiles in detail. Thus, it is important that we investigate oceanographic structure and water properties at the region of the Kerguelen Plateau as a part of circulation of AABW at the Southern Indian Ocean.

We provided an observation line crossing the Kerguelen Plateau and carried out Conductivity–Temperature–Depth profilers (CTD) and Lowered Acoustic Doppler Current Profilers (LADCP) observations by Training and Research Vessel Umitaka-Maru in February 2003. In this paper we first describe water mass property from hydrographic data, and then current distribution by LADCP. Finally, we discuss the velocity field and transport of results and conclude with a brief summary.

2. DATA

Hydrographic observation points (Fig. 1) were provided along the line (A-Line) crossing the Kerguelen Plateau followed the study of SPEER and FORBES (1994). The T/R Vessel Umitaka-Maru departed from Port Luis on 3

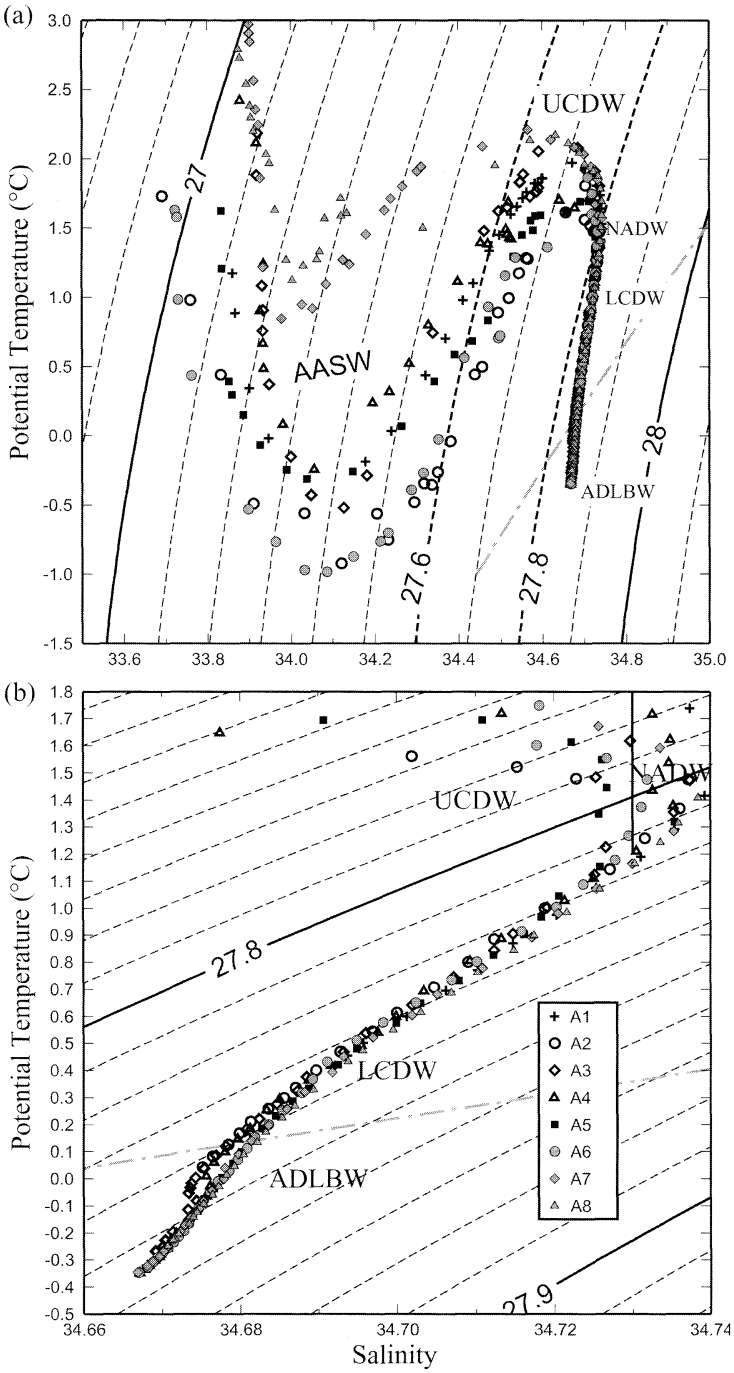

Fig. 2. Potential temperature (℃) −salinity relation of sea water for (a) whole water and (b) that for deep water. Each station is distinguished by a different symbol shown in the legend. The broken and solid lines indicate contours of constant potential density (σ_θ). Isopycnal of σ_θ=27.8 is the boundary of LCDW and UCDW, and follows the saltiest NADW (S>34.73: vertical solid line in (b)). Isopycnal of σ_θ=27.6 indicates the boundary of AASW and UCDW. Dash-dotted line indicates isopycnal of σ_4=46.04 as the boundary of LCDW and ADLBW (AABW).

January 2003, and arrived at the first observation point (Station A1) on 9 January. Observations from Station A1 to Station A8 were carried out for three days.

Temperature and salinity were measured by using Sea-Bird Electronics CTD. Salinity of bottle samples water were measured by using the Guildline AUTOSAL. Then, the conductivity sensor of CTD was calibrated against these bottle samples salinity data. Potential temperature (θ), density in situ (σ_t), potential density (σ_θ) and density at 4000 dbar (σ_4) were calculated from the pressure, the temperature and the calibrated salinity by using the equation of state, UNESCO (1981).

Ocean current velocity was measured by using LADCP, produced by RD Instruments, placed in the frame of CTD. The direction data of LADCP were corrected with International Geomagnetic Field Model 2000, because the current direction data measured by magnetic compass placed in LADCP have azimuth deviation from that by gyrocompass. Next, in order to minimize the effect of CTD motion, we got rid of the data when pitching or rolling is greater than 5 degree. Finally, zonal and meridional velocities are estimated by inverse solutions (VISBECK, 2000) every 20 dbar vertically.

3. Results

3.1 Water properties

Fig. 2 shows potential temperature-salinity relation for each station. The low salinity water covered the surface layer, are known as the Antarctic Surface Water (AASW) defined for the water properties of salinity (S) less than 34.0 with potential temperature (θ) $-1.84℃ < \theta < 2.00℃$ (BINDOFF *et al.*, 2000) or potential density (σ_θ) less than 27.6 (ORSI *et al.*, 1999). The cold AASW ($\theta < 0.5℃$) is found between Station A1 and Station A5, but not at Station A7 and Station A8; the difference between warmer and colder classes of AASW are easily seen on Fig. 2 (a) in the potential density ($27.2 < \sigma_\theta < 27.6$).

Below AASW, the warm and saline water mass that occupies most of the deep layers above the Antarctic Bottom Water (AABW) is the Circumpolar Deep Water (CDW). In the layer of CDW, the saltiest water (S>34.73) originated from the North Atlantic Deep Water (NADW) is found at all stations except at Station A5 as also shown in Fig. 3 (b). SPEER and FORBES (1994) suggested that the salinity field was dominated by the salinity maximum of old NADW. The isopycnal of σ_θ=27.79 (ORSI *et al.*, 1995; REID, 1989) or σ_θ=27.80-27.81 (HEYWOOD *et al.*, 1999) follows about the salinity maxima of the NADW that enters the ACC from the north in the southwestern Atlantic Ocean (REID, 1989). Water column is classified into the upper layer and the lower layer characterized Upper CDW (UCDW) and Lower CDW (LCDW), respectively (SPEER and FORBES, 1994). Details are shown in section 3.2.

Next, in bottom water, the Antarctic Bottom Water (AABW) whose salinity (S) is $34.65 < S < 34.72$ at potential temperature (θ) of $-0.4℃ < \theta < 0.0℃$ (BINDOFF *et al.*, 2000) and $\sigma_4 > 46.04$ (ORIS *et al.*, 1999) is distributed at all stations except Station A1. A little warmer and fresher water mass ($-0.1℃ < \theta < 0.5℃$) is located between Station A2 and Station A4 (near the Kerguelen Plateau) is different from that is located between Station A5 and Station A8 (near the South Indian Basin). This difference is due to the fact that the water of the shore region is fresher and warmer than that of the basin region. In contrast, the property is same in the deeper region from Station A2 to Station A8 at the potential temperature colder than $-0.1℃$.

RODMAN and GORDON (1982) indicated that the property of AABW in the eastern side of Kerguelen Plateau was different from that in the western side, and the potential source of Weddell Sea Bottom Water from the Weddell-Enderby Basin across the Princess Elisabeth Trough is negligible. The AABW whose salinity is lower than 34.68 formed off Adélie Land (ADLBW: Adélie Land Bottom Water) flows cyclonically along the southern and western rims of the South Indian Basin (MANTYLA and REID, 1995). ORSI *et al.* (1999) defined the bottom water the coldest and freshest ($\theta < -1.0$ ℃ and S<34.64) in the southwestern Weddell Sea, the warmest and saltiest ($-0.6℃ < \theta < 0.3$ ℃ and S>34.72) in the northwestern Ross Sea, and the intermediate properties ($-0.8℃ < \theta < -0.4℃$ and $34.62 < S < 34.68$) off the Adélie

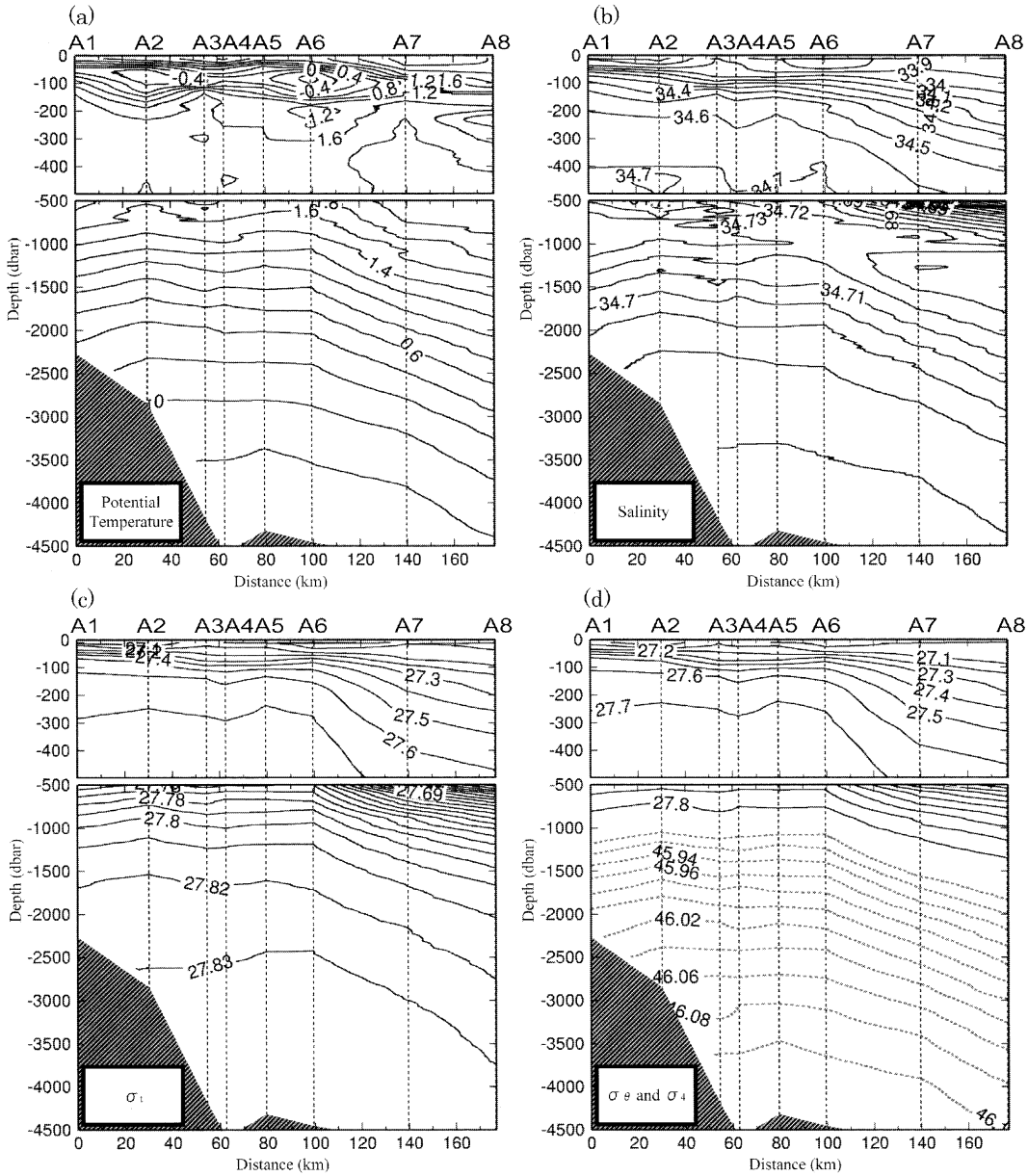

Fig. 3. Vertical sections of (a) potential temperature in ℃, (b) salinity, (c) σ_t and (d) σ_θ (solid lines) or σ_4 (dotted lines). Vertical broken lines indicate observation stations; station numbers are indicated above the plots.

Land (140°–150°E). The AABW in this observation indicates same properties of that off the Adélie Land (ADLBW) by ORSI *et al.* (1999). Moreover, BINDOFF *et al.* (2000) also defined that property of ADLBW was θ <0.5℃ at salinity 34.66<S<34.68, and the sea water is in the present study.

Comparing the properties of AABW in this observation with that in the previous observations mentioned above, there are slight differences in the water properties. ORSI *et al.* (1999) indicated that deep water properties in this

region was $\theta = -0.5$℃ and S>34.67 at the bottom. SPEER and FORBES (1994) also described that the deepest water properties converged on $\theta = -0.5$℃ and S=34.675 to the bottom. But the water property is a little warmer and saltier. SPEER and FORBES (1994) indicated that observed AABW was warmer and saltier than that of previous observation by GORDON *et al.* (1982) at the same density field below 0℃. Consequently, we compare the water properties by SPEER and FORBES (1994) (referred by their Fig. 5) with those in our observation (Fig. 2). In so far as what we compare these figures at the same density field below 0.0℃, the AABW in our observation is a little warmer and fresher than that by SPEER and FORBES (1994), and is almost similar to that by GORDON *et al.* (1982). SPEER and FORBES (1994) assumed the difference suggesting that the AABW sources varied along the southern boundary off the Antarctic as far east as the Ross Sea with the time scale of 20 years or less. Nevertheless their assumption remains a matter for speculation; the differences mentioned above are possible due to the historical changes.

3.2 Distribution of water mass

Fig. 3 shows vertical distribution of potential temperature, salinity, σ_t and σ_θ or σ_4. The water mass colder than 0.0℃ is distributed near 70dbar between Station A1 and Station A6 as shown in Fig. 3 (a). This water is the coldest in this region; the temperature is lower than −0.4℃ between Station A2 and Station A3, especially lower than −0.8℃ at Station A6. In addition, a couple of lens-like temperature structure exists about 70 dbar depth between Station A1 to Station A6. This coldest water is not distributed between Station A7 and Station A8. The contrast between two groups also can be clearly seen in Fig. 2 (a). The warmest water lies around 500 dbar depth. ORSI *et al.* (1995) described that at the position of the southern ACC front there is a distinct temperature gradient along the θ-maximum of the UCDW, as it shoals southward to near 500 dbar (θ>1.8℃). As the water property distribution is clearly different between Station A6 and Station A7, the existence of the southern ACC front is suggested.

The Kerguelen Plateau (70°-80° E) clearly obstructs the path of the southern ACC front and forces it farther to the south (ORSI *et al.*, 1999). East of the plateau, the southern ACC front turns sharply to the north forming a boundary current along its eastern flank (RODMAN and GORDON, 1982; SPEER and FORBES, 1994). Sparrow *et al.* (1996) suggested by Fine Resolution Antarctic Model (FRAM) that the southern ACC front moved northward along the eastern side of the Kerguelen Plateau to about 55° S. ORSI *et al.* (1995) described that property indicators of the southern ACC front were θ>1.8℃ along θ-maximum at the depth deeper than 500 dbar farther north of the front, or θ<0.0℃ along θ-minimum at the depth shallower than 150 dbar farther south of the front. Such water properties are found between Station A6 and Station A7.

Next, as shown in Fig. 3 (b), strong halocline with θ<0.0℃ is found at 70 dbar depth between Station A1 and Station A6. The saltiest water is distributed around 500 dbar depth at Station A1. On the other hand, it is found around 1200 dbar depth at Station A8. Accordingly, a strong salinity gradient exists between 500 dbar and 1200 dbar. This gradient also indicates the existence of the southern ACC front.

Finally we describe the density distribution. As shown in Figs. 3 (c) and (d), the strong pycnocline exists in the layer around 50 dbar between Station A1 and Station A6. In addition, a lens-like structure is conspicuous around this depth between Station A3 and Station A5, and suggests an existence of cyclonic eddy in this region. The strong horizontal gradient is also found in the density field below 100 dbar off shore of Station A6. This suggests that the southward flow exists off the southern ACC front. In contrast, a weak but opposite density gradient in the near-shore region is remarkable. This means an existence of northward flow.

We reconsider the previously described water distribution from the perspective of water property.

The coldest water in this region has the property of the Antarctic Surface Water (AASW) (−1.84℃< θ <2.00℃, S<34.00) (BINDOFF *et al.*, 2000). Below the AASW, UCDW (27.35< σ_θ

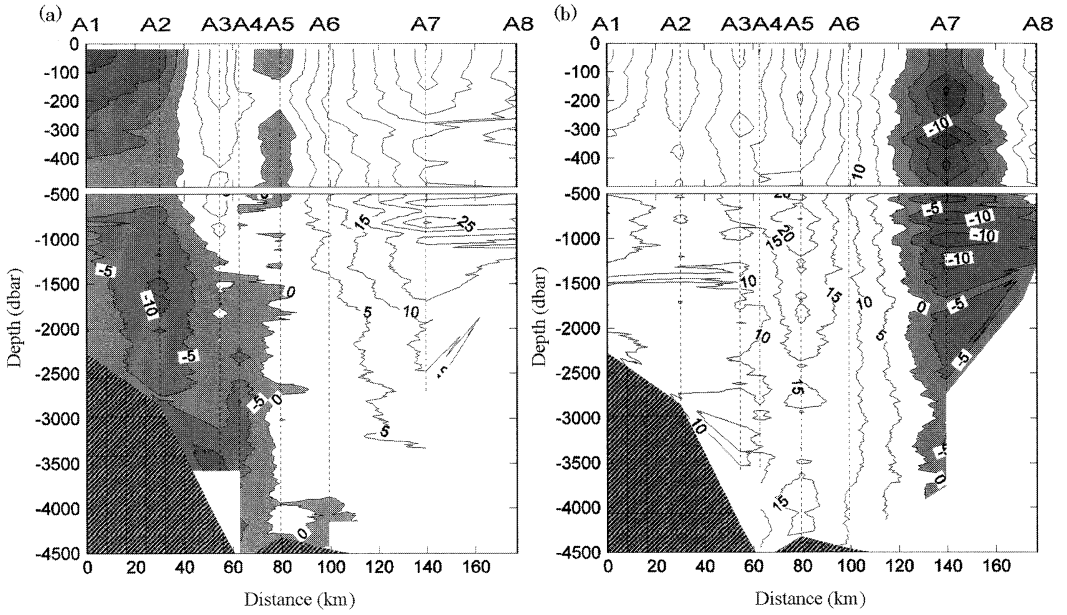

Fig. 4. Vertical sections of (a) eastward and (b) northward current velocity in cm/s measured by LADCP. Contour interval is 5 cm/s. Shaded areas indicate (a) westward and (b) southward current. Locations of observation stations are the same as these in Fig.3.

<27.75) (SIEVERS and NOWLIN, 1984) lies between 100 and 1000 dbar. According to the previous studies, the isopycnal of σ_θ=27.79 (ORSI *et al.*, 1995; REID, 1989) or σ_θ=27.80–27.81 (HEYWOOD *et al.*, 1999) follows the saltiest NADW. In this observation, the saltiest water mass is found around the isopycnal σ_θ=27.80. This isopycnal lies around 700 dbar between Station A2 and Station A6, and lies around 1000 dbar between Station A7 and Station A8. Below UCDW, the LCDW lies above AABW about 2500dbar. ORSI *et al.* (1999) adopted the σ_4=46.04–46.06 (Fig. 3 (d)) as a boundary between LCDW and AABW (ADLBW). ADLBW (θ <0.5 ℃ and 34.66<S<34.68) defined by BINDOFF *et al.* (2000) is found between Station A2 and Station A8 below LCDW.

3.3 Structure of the boundary current

In the vertical distribution of current shown in Fig. 4, the northwestward boundary current exists between Station A1 and Station A4 over the continental slope. Below 500 dbar, the westward current speed higher than 10 cm/s is observed around 1500 dbar depth at Station A2, and around 3500 dbar depth at Station A3. Current flows almost along isobaths between Station A1 and Station A4, although the direction is northeastward above about 1500 dbar between Station A3 and Station A4. Moreover northward flow is observed at Station A5 from bottom to surface, and northeastward extends from Station A5 to Station A6. Such a complicate current structure suggests the existence of a cyclonic eddy, which is already found as a lens-like structure in temperature and density field between Station A1 to Station A5.

The northward current speed is the highest at Station A5, and averaged current speed from surface to bottom is about 19 cm/s. DONOHUE *et al.* (1998) already pointed out that the core of northward boundary current existed around there. Current direction changes from northward to southward from bottom to surface between Station A6 and Station A7 where the southern ACC front exists. The Southward current velocity is more than 30 cm/s at 700 dbar of Station A7.

3.4 Geostrophic volume transport

Evaluating geostrophic current, it is important that the current velocity at the reference

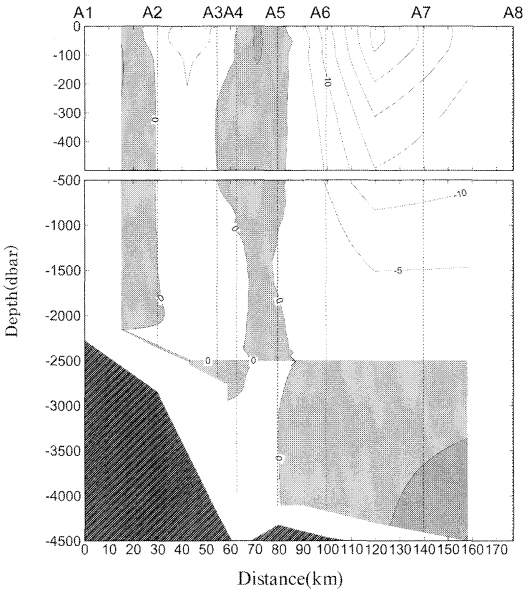

Fig. 5. Vertical section of the geostrophic current in cm/s for the reference level of 2500 dbar between Station A2 and Station A8. The deepest common depth of 2157 dbar is used between Station A1 and Station A2. Shaded areas indicate the northwestward current. Contour interval is 5 cm/s. Locations of observation stations are the same as these in Fig.3.

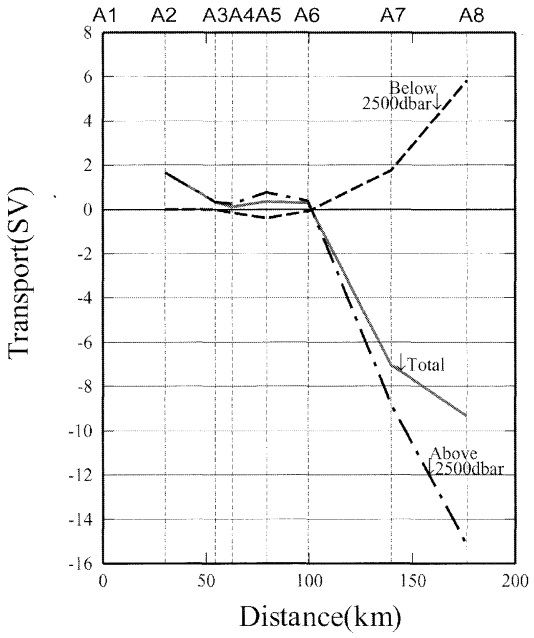

Fig. 6. Cumulative geostrophic transports integrated from Station A1 to Station A8. Positive value indicates the northwestward transport. Solid, dash-dotted and broken lines indicate the transport between surface and bottom (total), above 2500 dbar and below 2500 dbar, respectively.

level is negligible (SPEER and FORBES, 1994). They estimated northwestward geostrophic transports taking a reference at 2500 dbar depth, and obtained the transport of −12 SV (1 SV=10^6 m^3/s) between the reference level and the surface, 6 SV between the reference level and the bottom, and −6 SV in total. We first follow their analysis and choose 2500 dbar depth taking a reference level, and then, compare the current fields and transports by geostrophic calculation taking a reference of level of no motion with those by the direct current observations of LADCP.

As shown in Fig. 5, above the reference level, the northwestward currents are estimated between Station A1 and Station A2, and between Station A4 and Station A5. In contrast to this, southeastward current is estimated between Station A2 and Station A3. Above the reference level, the strong southeastward current is estimated between Station A5 and Station A8, and is larger than 30 cm/s at between Station A6 and Station A7 above 70 dbar. Below the reference level, northwestward current is estimated at between Station A6 and Station A7. The integrated transport (Fig.6) from Station A1 to Station A6 is about 0 sv above and below the reference level (2500 dbar), and much smaller than that between Station A6 and Station A8 (Table. 1). The transport on the plateau between Station A1 and Station A6 is smaller than that obtained by SPEER and FORBES (1994), because the northward transport associated with the cyclonic eddy prevails between Station A2 and Station A3. Northwestward transport exists between Station A6 and Station A8 below the reference level. Comparing this transport with their resolution; our estimate between Station A6 and Station A8 is about 6 SV, and coincided with their estimate (referred to their Fig. 4; the integrated transport of northeastern part about 100 km from reversals of transport below reference level, SPEER and FORBES, 1994).

We compare geostrophic transport taking a reference of level of no motion at 2500 dbar

Table. 1. Northwestward geostrophic transports in Sv (1 SV=10^6 m^3/s) below 2500 dbar, above 2500 dbar and between surface and bottom, respectively, as function of station (row) and geostrophic reference technique (column).

	A1–A6	A6–A8	A1–A8(total)
	from surface to bottom		
LNM*	0.2	−9.5	9.3
LADCP**	38.0	−39.5	−1.5
	above 2500 dbar		
LNM*	0.3	−15.5	−15.2
LADCP**	28.0	−31.5	−3.5
	below 2500 dbar		
LNM*	−0.1	6.0	5.9
LADCP**	10.0	−8.0	2.0

* Taking a reference of a Level of no motion at 2500 dbar.

** Matching geostrophic transport with that measured by LADCP between adjacent stations.

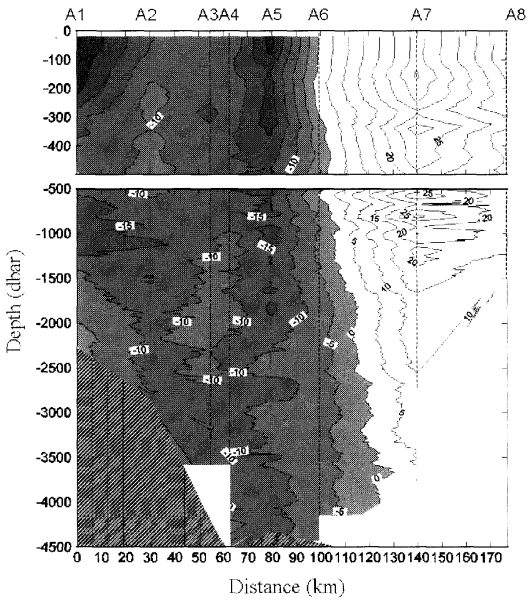

Fig. 7. Vertical section along the section (A-line) of current in cm/s observed by LADCP. Contour interval is 5 cm/s. Shaded areas indicate the northwestward current. Locations of observation stations are the same as these in Fig. 3.

(Fig. 5) with LADCP data (Fig. 7). The geostrophic transport taking a reference of level of no motion indicates that the the northwestward current is located between Station A6 and Station A8. On the other hand, direct current observations of LADCP the

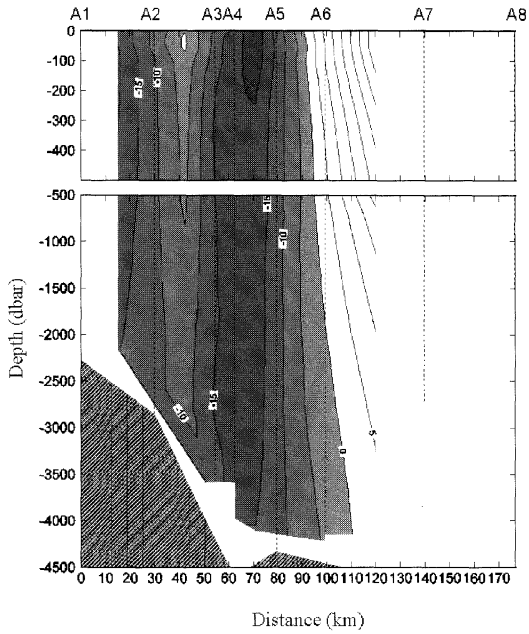

Fig. 8. Vertical section of the geostrophic current velocity in cm/s. The current is estimated by matching its total transport with that measured by LADCP between adjacent stations. Contour interval is 5 cm/s. Shaded areas indicate the northwestward current. Locations of observation stations are the same as these in Fig. 3.

northwestward current indicated that DWBC is located between Station A1 and Station A6.

The estimates based on a level of no motion are only based on the baroclinic flows referring to structure of density fields. DONOHUE *et al.* (1998) also suggested that the geostrophic transports based on a level of no motion would consequently underestimate the transport in the DWBC. Geostrophic calculations only yield velocity shear, and knowledge of the absolute velocity at any depth is required to estimate the barotropic component (HEYWOOD *et al.*, 1999).

Thus, in the present analysis, the geostrophic transport is estimated by matching its total transport with that by LADCP data between adjacent stations (Fig. 8). The current distribution shown in Fig. 9 is almost similar to these by the direct current observations of the LADCP as shown in Fig. 8. The integrated transport from Station A1 to Station A6 measured by the LADCP is about 10.0±1.3

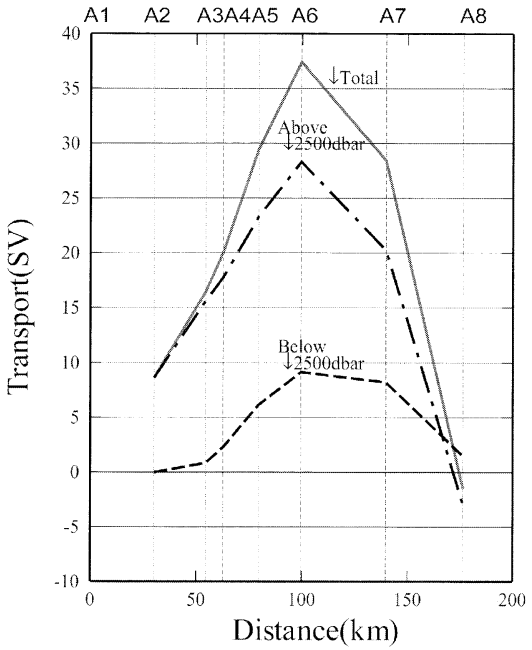

Fig. 9. Cumulative transports by cross-section LADCP velocity integrated from Station A1 to Station A8. Positive value indicates the northwestward transport. Solid, dash-dotted and broken lines indicate the transport between surface and bottom (total), above 2500 dbar and below 2500 dbar, respectively.

SV (Table. 1). As mentioned above, SPEER and FORBES (1994) and we estimate the DWBC transport at 6.0 SV based on the level of no motion at 2500 dbar. Thus, our own estimate is about 1.7 times larger than that by theirs. In addition, the DWBC is located between Station A6 and Station A8 by the geostrophic transport estimate taking a reference of no motion at 2500 dbar (Fig. 5), but that exist between Station A1 and Station A6 by the direct current observations of LADCP (Fig. 7).

4. Discussion

In consequence of matching the geostrophic fields to direct current observations by using LADCP, we can estimate the barotropic and baroclinic transports of DWBC. Barotropic transports are evaluated by the surface flow of the geostrophic current between adjacent stations by the method mentioned above. The barotropic and baroclinic transports between Station A6 and Station A7 are about 19.3 SV northwestward and 40.3 SV southeastward, respectively, and show that the southeastward transport of the ACC at the northern region of the southern ACC front. The northwestward barotropic and baroclinic transports are negligible and 4.3 SV between Station A2 and Station A3, and 4.4 SV and 1.0 SV between Station A3 and Station A4, respectively. This indicates the evidence of eastward flow due to the clockwise vortex around these stations. This vortex also appears in the distribution of temperature, salinity and density fields. A couple of lens-like structure of temperature exists about 70 dbar between Station A1 and Station A6. In this region around 70 dbar, the constricted part of temperature is located between Station A3 and Station A4 and distributes saline and high-density water; fresher and low-density water is distributed in the other region. The barotropic and baroclinic transports estimated are at 15.2 SV northwestward and 5.2 SV southwestward, respectively, between Station A1 and Station A6 below 2500 dbar where the DWBC exists. Accordingly, the geostrophic calculation based on the level of no motion at the 2500 dbar gives transports smaller than that based on direct current measurement by LADCP, because the barotropic transport at the level is not taken into account.

DONOHUE *et al.* (1998) used the method similar to that in present study and estimated transport below 500 dbar where potential temperature is lower than 1.0℃. They estimated the northwestward transport of 48.9±9.4 SV. Our calculation for the same temperature range and obtained the northwestward transport of 22.3±4.1 SV, which is less than a half of their estimation. Unfortunately, we cannot compare the current distribution directly with theirs, because they do not show the distribution in detail. But one of the reasons of the difference is probably due to difference of the observation line and period.

Acknowledgments

We would like to thank the captain Yoshio Koike, officers, crew and scientists of 9th cruise of the T/R Vessel Umitaka-Maru of Tokyo University of Marine Science and Technology from Port Luis to Fremantle. The

hydrographic observations are supported by any scientists, especially, the primary researcher of doctor Takashi Ishimaru. We also thank doctor Masao Nemoto for helpful discussions. We are very grateful to reviewer for their fruitful and constructive comments. Logistical support was provided by a Grant-in-Aid for Scientific Research (A) (14255012) from Japan Society for the Promotion of Science (JSPS).

References

BINDOFF, N.L., M.A. ROSENBERG and M.J. WARNER (2000) : On the circulation and water masses over the Antarctic continental slope and rise between 80 and 150° E. Deep-Sea Res. II, **47**, 2299-2326.

DONOHUE, K.A., G.E. HUFFORD and M.S. MCCARTNEY (1998) : Sources and transport of the Deep Western Boundary Current east of the Kerguelen Plateau. Geophys. Res. Lett., **26** (**7**), 851-854.

GORDON, A.L., E.J. MOLINELLI, and T.N. BAKER (1982): Southern Ocean Atlas. Columbia University Press, New York, 34pp

HEYWOOD, K.J., M.D. SPARROW, J. BROWN and R.R. DICKSON (1999) : Frontal structure and Antarctic Bottom Water Flow through the Princess Elizabeth Trough, Antarctica. Deep-Sea Res. I, **46**, 1181–2000.

MANTYLA, A.W. and J.L. REID (1995) : On the origins of deep and bottom waters of the Indian Ocean. J. Geophys. Res., **100**, 2417–2439.

ORSI, A.H., G.C. JOHNSON, and J.L. BULLISTER (1999): Circulation, mixing and the production of Antarctic Bottom Water. Prog. Oceanogr., **43**, 55–109.

ORSI, A.H., T. WHITEWORTH III and W.D. NOWLIN Jr., (1995) : On the meridional extent and fronts of the Antarctic Circumpolar Current. Deep-Sea Res. I, **42**, 641–673.

REID, J.L. (1989) : On the total geostrophic circulation of the South Atlantic Ocean: flow pattern, tracers and transports. Prog. Oceanogr., **23**, 149–244.

RODMAN, M.R., and A.L. GORDON (1982) : Southern Ocean bottom water of the Australian-New Zealand sector. J. Geophys. Res., **87**, 5771–5778.

SIEVERS, H.A. and W.D. NOWLIN Jr., (1984) : The stratification and water masses at Drake Passage. J. Geophys. Res., **89** (**C6**), 10489–10514.

SPARROW, M.D., K.J. HEYWOOD, J. BROWN and D.P. STEVENS (1996) : Current structure of the South Indian Ocean. J. Geophys. Res., **101**, 6377–6392.

SPEER, K.G., and A. FORBES (1994) : A deep water boundary current in the Indian Ocean. Deep-Sea Res. I, **41**, 1289–1303.

UNESCO (1981) : Tenth report of the joint panel on oceanographic tables and standards. UNESCO Technical Papers in Marine Science, Number 36, UNESCO, Paris, 1–45.

VISBECK, M. (2000) : Deep Velocity Profiling using Lowered Acoustic Doppler Current Profiler: Bottom Track and Inverse Solutions. J. Ocean. Tech., **19** (**5**), 794–807.

Received June 28, 2005
Accepted September 16, 2005